

First-principles study of non-radiative carrier capture by defects at amorphous-SiO_2/Si(100) interface

Haoran Zhu(祝浩然), Weifeng Xie(谢伟锋), Xin Liu(刘欣), Yang Liu(刘杨),Jinli Zhang(张金利), and Xu Zuo(左旭)
Citation: Chin. Phys. B, 2023, 32 (**7**): 077303. DOI: 10.1088/1674-1056/ac9fc2
Journal homepage: http://cpb.iphy.ac.cn; http://iopscience.iop.org/cpb

What follows is a list of articles you may be interested in

Ozone oxidation of 4H-SiC and flat-band voltage stability of SiC MOS capacitors

Zhi-Peng Yin(尹志鹏), Sheng-Sheng Wei(尉升升), Jiao Bai(白娇), Wei-Wei Xie(谢威威), Zhao-Hui Liu(刘兆慧), Fu-Wen Qin(秦福文), and De-Jun Wang(王德君)
Chin. Phys. B, 2022, 31 (**11**): 117302. DOI: 10.1088/1674-1056/ac7ccf

Surface modulation of halide perovskite films for efficient and stable solar cells

Qinxuan Dai(戴沁煊), Chao Luo(骆超), Xianjin Wang(王显进), Feng Gao(高峰), Xiaole Jiang(姜晓乐), and Qing Zhao(赵清)
Chin. Phys. B, 2022, 31 (**3**): 037303. DOI: 10.1088/1674-1056/ac1fe0

Interface and border trapping effects in normally-off Al_2O_3/AlGaN/GaN MOS-HEMTs with different post-etch surface treatments

Si-Qi Jing(荆思淇), Xiao-Hua Ma(马晓华), Jie-Jie Zhu(祝杰杰)†, Xin-Chuang Zhang(张新创), Si-Yu Liu(刘思雨), Qing Zhu(朱青), and Yue Hao(郝跃)
Chin. Phys. B, 2020, 29 (**10**): 107302. DOI: 10.1088/1674-1056/ab99bb

Negative bias-induced threshold voltage instability and zener/interface trapping mechanism in GaN-based MIS-HEMTs

Qing Zhu(朱青), Xiao-Hua Ma(马晓华), Yi-Lin Chen(陈怡霖), Bin Hou(侯斌), Jie-Jie Zhu(祝杰杰), Meng Zhang(张濛), Mei Wu(武玫), Ling Yang(杨凌), Yue Hao(郝跃)
Chin. Phys. B, 2020, 29 (**4**): 047304. DOI: 10.1088/1674-1056/ab7809

Effect of PECVD SiN_x/SiO_yN_x-Si interface property on surface passivation of silicon wafer

Xiao-Jie Jia(贾晓洁), Chun-Lan Zhou(周春兰), Jun-Jie Zhu(朱俊杰), Su Zhou(周肃), Wen-Jing Wang(王文静)
Chin. Phys. B, 2016, 25 (**12**): 127301. DOI: 10.1088/1674-1056/25/12/127301

First-principles study of non-radiative carrier capture by defects at amorphous-SiO_2/Si(100) interface

Haoran Zhu(祝浩然)[1], Weifeng Xie(谢伟锋)[1], Xin Liu(刘欣)[1], Yang Liu(刘杨)[2,3], Jinli Zhang(张金利)[1], and Xu Zuo(左旭)[1,4,5,†]

[1] *College of Electronic Information and Optical Engineering, Nankai University, Tianjin* 300350, *China*
[2] *Institute of Electronic Engineering, China Academy of Engineering Physics, Mianyang* 621999, *China*
[3] *Microsystem and Terahertz Research Center, China Academy of Engineering Physics, Chengdu* 610200, *China*
[4] *Key Laboratory of Photoelectronic Thin Film Devices and Technology of Tianjin, Nankai University, Tianjin* 300350, *China*
[5] *Engineering Research Center of Thin Film Optoelectronics Technology, Ministry of Education, Nankai University, Tianjin* 300350, *China*

(Received 20 August 2022; revised manuscript received 1 November 2022; accepted manuscript online 3 November 2022)

Defects have a significant impact on the performance of semiconductor devices. Using the first-principles combined with one-dimensional static coupling theory approach, we have calculated the variation of carrier capture coefficients with temperature for the interfacial defects P_{b0} and P_{b1} in amorphous-SiO_2/Si(100) interface. It is found that the geometrical shapes of P_{b0} and P_{b1} defects undergo large deformations after capturing carriers to form charged defects, especially for the Si atoms containing a dangling bond. The hole capture coefficients of neutral P_{b0} and P_{b1} defects are largest than the other capture coefficients, indicating that these defects have a higher probability of forming positively charged centres. Meanwhile, the calculated results of non-radiative recombination coefficient of these defects show that both P_{b0} and P_{b1} defects are the dominant non-radiative recombination centers in the interface of a-SiO_2/Si(100).

Keywords: interface defect, carrier capture coefficients

PACS: 73.50.Gr **DOI:** 10.1088/1674-1056/ac9fc2

1. Introduction

Around the world, silicon dioxide (SiO_2) is a common component of sands. In microelectronic systems, amorphous silicon dioxide (a-SiO_2) is used as an insulating layer. Charge capture by defects in the SiO_2 and transition layers is a critical problem that must be addressed in order to improve semiconductor device dependability. Unlike defects in bulk a-SiO_2, when defects capture charge carriers at the interface of a-SiO_2 and Si (a-SiO_2/Si), it will be difficult to recover electric neutrality, causing device performance to deteriorate and eventually leading to device failure.[1–4] Unsaturated dangling bonds, also known as P_b-type defects found at the a-SiO_2/Si interface are the major electronically active defects, are located in the interface of a-SiO_2/Si and are detected using the electron spin-resonance (ESR) spectroscopy[5–8]. The P_b defect is discovered at a-SiO_2/Si(111), with its isolated sp^3 hybrid dangling bond oriented in the (111) direction, orthogonal to the interface[5]. Other two unique defects, P_{b0} and P_{b1}, which are situated in the technologically important (100) interface, with isolated sp^3 hybrid dangling bonds pointing in the directions of (111) and (211), respectively.[2,8] Because the capture and accumulation of carriers to these defects cause the gate voltage to change and acts as non-radiative recombination sites to diminish the minority carrier density, understanding the microscopic mechanism of carrier capture and identifying dominant defects is crucial.[9,10] Unlike point defects in a-SiO_2, interface traps seldom anneal at ambient temperature and continue to interfere with device function.[9]

Because direct measurement of the carriers capture process is challenging experimentally, especially in terms of identifying relevant defects, it is vital to investigate the related phenomena using theoretical calculations based on an *ab initio* technique.[11,12] The adiabatic approximation,[13] Marcus theory,[14] quantum charge transfer theory[15] and static coupling theory[16–18] have been used to construct the electron–phonon coupling matrix, which determines the carriers capture properties of defects. Recently, Alkauskas *et al.*[18] established a method for calculating the electron–phonon coupling matrix using a one-dimensional (1D) configuration coordinate for the effective vibrational wave function and static coupling theory. This theory was applied to many hole capture defects in GaN and ZnO, and the hole capture coefficients found are consistent with experiment data. Therefore, in our work, we investigate the non-radiative carrier capture coefficients of the P_{b0} and P_{b1} defects using this 1D static coupling theory. Our results indicate that the P_{b0} and P_{b1} defects form positive centers more easily than negatively charged defect centers, and are indeed non-radiative recombination center in the interface of a-SiO_2/Si(100).

2. Theoretical method

The spin-polarized first-principles calculations are performed in the Vienna *ab initio* simulation package (VASP)[19,20] with projector-augmented-wave (PAW)

†Corresponding author. E-mail: xzuo@nankai.edu.cn

© 2023 Chinese Physical Society and IOP Publishing Ltd

pseudopotentials.[21] Generalized gradient approximation (GGA) in the Perdew–Burke–Ernzerhof (PBE) form[22,23] is used for the optimization of geometrical structure and a cutoff energy of 500 eV for the plane-wave expansion is adopted. The convergence criteria are 10^{-5} eV and 0.01 eV·Å^{-1} for energy and force, respectively. The structure models of P_{b0} and P_{b1} defects are obtained by Li *et al.*,[24] with a dimension of 15.4 Å × 15.4 Å × 35.0 Å. Hybrid functional based on the Heyd–Scuseria–Ernzerhof (HSE06) method[25] is employed to obtain the exact electronic properties.

The formation energy (E_f) of defect X in charge state q is calculated by

$$E_f[X^q] = E_{tot}[X^q] - E_{tot}[\text{bulk}] - \sum_i n_i\mu_i + q(\varepsilon_F + \Delta V_{VBM}) + E^q_{corr}, \quad (1)$$

where $E_{tot}[X^q]$ and $E_{tot}[\text{bulk}]$ are the energies of system with defect X in charge state q and without defect, respectively. n_i is the atomic number that should add (>0) or remove (<0) from pure system to construct defect X, μ_i is the chemical potential of atom μ, ε_F is Fermi energy relative to the valence band maximum (VBM), E^q_{corr} is correction term for charged system, proposed by Refs. [24,26] by using finite element method.

The E^q_{corr} is the change in electrostatic energy from the periodic boundary condition ($E_{periodic}$) to the open boundary condition ($E_{isolated}$) for an isolated defect with charge q[27]

$$E_{corr} = E_{isolated} - E_{periodic} + q\Delta V, \quad (2)$$

where the last term is an alignment term of the classical electrostatic calculation to that of the DFT calculation.[28]

The finite element method is employed to correct the formation energy, and the charge density and dielectric constant profile of interface defects are extracted from the first principles calculations.[24] The defect charge is approximated by a Gaussian distribution. The Gaussian distribution is defined for the periodic boundary condition as[27]

$$\rho_{periodic}(r) = \frac{qQ_0}{\sigma^3(2\pi)^{3/2}} e^{-r^2/(2\sigma^2)} - \frac{qQ_0}{\Omega}, \quad (3)$$

where σ is the standard deviation, which defines the localization of the defect wave function, $Q_0 = 1.6 \times 10^{-19}$ C is the elementary charge, and q is the charge of the defect. The uniform background charge density of qQ_0/Ω is added to obtain better convergence under the periodic boundary condition, and Ω is the volume of the simulation unit cell. Under the ground boundary condition and without the uniform charge background, Eq. (3) can be written as

$$\rho_{ground}(r) = \frac{qQ_0}{\sigma^3(2\pi)^{3/2}} e^{-r^2/(2\sigma^2)}. \quad (4)$$

The permittivity profile can be obtained by polarizabilities of atoms, which include the electronic polarizabilities (α_{elec}) and the ionic polarizabilities (α_{ion}).[29] The static permittivity can be written as

$$\varepsilon_0 = 1 + \frac{4\pi}{\Omega}\sum(\alpha_{elec} + \alpha_{ion}), \quad (5)$$

where polarizabilities α_{elec} and α_{ion} of Si atoms in different oxidation states can be obtained in Ref. [29]. A normalized Gaussian smearing function is multiplied to each atomic effective polarizability to smooth the permittivity profile. Thus, the permittivity profile along the z-axis is defined as

$$\varepsilon(z) = 1 + \frac{4\pi}{\Omega}\sum\frac{(\alpha^i_{elec} + \alpha^i_{ion})}{\sigma(2\pi)^{1/2}} e^{-(z-z_i)^2/(2\sigma^2)}, \quad (6)$$

where $\alpha^i_{elec} + \alpha^i_{ion}$ is the polarizability of the i-th Si atom at the z-position z_i, and the standard deviation σ is chosen to be 1.4 Å, which is the distance between two adjacent Si planes along the [001] direction, and the permittivity profile can be found in Ref. [24].

The electrostatic potential $V(r)$ is the solution of the Poisson equation $\nabla\cdot[\varepsilon(r)\nabla V(r)] = -\rho(r)$, and the electrostatic energies $E_{periodic}$ and $E_{isolated}$ are calculated by solving $E = (1/2)\int V(r)\rho(r)\mathrm{d}r$ for the corresponding model electrostatic potential $V(r)$ under the respective boundary condition. It should be noted that the $E_{isolated}$ is obtained by scaling the simulation box uniformly.

Thus, the $+/0$ and $0/-$ charge-state transition levels calculated from the formation energy of Eq. (1) are given by

$$\varepsilon(+/0) = E_{tot}[X^0] - E_{tot}[X^+] - \Delta V^+_{VBM} - E^+_{corr}, \quad (7)$$

$$\varepsilon(0/-) = E_{tot}[X^-] - E_{tot}[X^0] - \Delta V^-_{VBM} + E^-_{corr}. \quad (8)$$

The relevant calculation results can be found in the supporting information.

Non-radiative carrier capture via multiphonon emission is a common phenomenon for deep defect levels in semiconductors. As shown in Fig. 1, the initial excited state of the defect vibrates around the equilibrium geometry. Owing to the electron–phonon coupling, the deformation of the structure will change the electronic state of the defect and form final ground state. Then, the final ground state will relax to the equilibrium structure due to phonon–phonon interactions, and the atomic relaxations are represented by a 1D configuration coordinate Q, the minima of the two potential energy surfaces are offset vertically by ΔE, which corresponds to the charge-state transition level, and horizontally by effective configuration coordinate ΔQ between the excited state and the ground state. According to the 1D static coupling theory, the corresponding capture coefficient is given by Alkauskas *et al.*[18]

$$C = V\frac{2\pi}{\hbar}gW^2_{if}\sum_m\omega_m\sum_n|\langle\xi_{im}|\Delta Q|\xi_{fn}\rangle|^2\delta(\Delta E + m\hbar\omega_i - n\hbar\omega_f), \quad (9)$$

where V is the volume of the supercell, and it will replace by S (the surface areas of the a-SiO_2/Si(100)) because we are

concerned with interface defects. g is the degeneracy factor (for a-SiO_2/Si(100), $g = 1$). W_{if}^2 is the elertron–phonon coupling matrix elements of initial and final states, ξ_{im} and ξ_{fn} are the vibrational wave function of initial excited state with vibrational frequency ω_i and final ground state with vibrational frequency ω_f, respectively, the vibrational frequency can be obtained by solving the 1D Schrödinger equation for potential energy surfaces around the equilibrium geometry. ω_m is the thermal occupation number of the initial excited vibrational state ξ_{im}, which determines the temperature-dependence of the capture coefficient, and ΔE corresponds to the energy of charge-state transition with respect to the VBM for hole capture and CBM for electron capture.

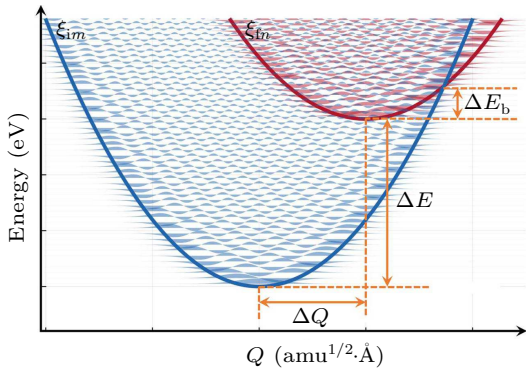


Fig. 1. Schematic of configuration coordinate for non-radiative carrier capture. The red and blue lines represent initial excited state with vibrational wave function ξ_{im} and final ground state with vibrational wave function ξ_{fn}, respectively. ΔE is the ionization energy of the defect, ΔE_b serves as a classic energy barrier of carrier capture, and Q is 1D effective configuration coordinate.

The degree of deformation is described by the 1D effective configuration coordinate ΔQ of initial and final states

$$\Delta Q^2 = \sum_{\alpha,t} m_\alpha \Delta R_{\alpha t}^2, \tag{10}$$

where m_α and $\Delta R_{\alpha t}$ are the mass and the displacement along the direction t from the equilibrium atomic coordinate of atom α, respectively.

The rationality of 1D static coupling theory is premised on Huang–Rhys factor $S \gg 1$, which corresponds to the large lattice relaxation associated with the change of the charge state, thus it is possible to replace the sum over all vibrational degrees of freedom with one special phonon model.[30] The S is defined as

$$S_{i,f} = \frac{1}{2\hbar}(\triangle Q)^2 \omega_{i,f}. \tag{11}$$

3. Results and discussion

3.1. Geometric structures and electronic properties of P_{b0} and P_{b1} defects

The concentration of the P_{b0} defect in the a-SiO_2/Si(100) interface is approximately 5×10^{12} cm^{-2},[32] located in the second Si layer near the interface. The P_{b0} defect is constructed primarily by removing a Si atom from the second layer of the interface on the Si side, resulting in four dangling bonds, three of which are saturated by H atoms, and the fourth dangling bond is the P_{b0} defect (Fig. 2(a)). In the case of the P_{b1} defect, which is located in the topmost layer of the Si side, the P_{b1} defect concentration in the a-SiO_2/Si(100) interface is around 1×10^{12} cm^{-2},[32] which is a fifth of the P_{b0} defect concentration but nevertheless significant. Three different models have been proposed to define the P_{b1} defect, including dimer, bridge and asymmetrically oxidized dimer (AOD) models.[32] The AOD model is the most likely candidate than the dimer and bridge models for the P_{b1} defect, because the full set of hyperfine parameters is found to agree closely with the experimental data,[24,31] so we only choose this model in our research to study the carrier capture properties of P_{b1} defect. In the AOD model, the two lower back bonds of the fully coordinated Si atom near the SiO_2 layer are oxidized (Fig. 2(b)). Due to the existence of dangling bonds, the neutral P_{b0} and P_{b1} defects have a magnetic moment of 1 μ_B.

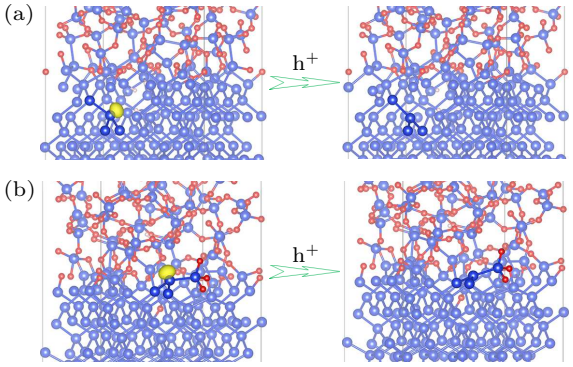


Fig. 2. The geometric structure of neutral (left) and positively charged (right) (a) P_{b0} defect and (b) P_{b1} defect.

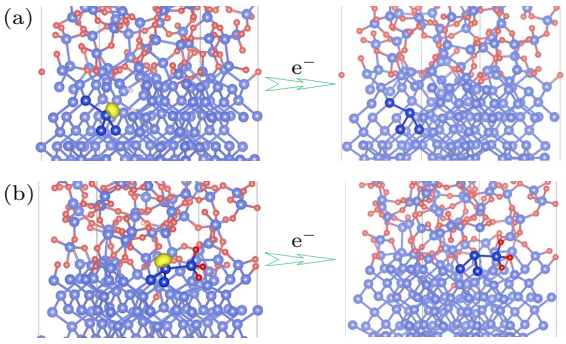


Fig. 3. The geometric structure of neutral (left) and negatively charged (right) (a) P_{b0} defect and (b) P_{b1} defect.

Table 1 shows the bond lengths and bond angles of the Si atom containing a dangling bond (Si_0) and the other three Si atoms coordinated to Si_0 at defect centers. When the defect captures a hole, the unpaired electron of the dangling bond along with the magnetic moment vanishes, and the defect structure tends to a plane structure similar to that of sp^2 hybridization (Fig. 2), resulting in shorter Si–Si bonds and larger ∠Si–Si–Si bond angles. However, for the P_{b1} defect, the bond length of the Si atom connecting to the three O atoms

(Si_{3O}) and Si_0 becomes longer due to the higher electronegativity of the O atom, which makes the type of bonding between O and Si between covalent and ionic bonds, resulting in different properties of Si_{3O}. In terms of electron capture, the dangling bond's unpaired electron would pair, and the magnetic moment would vanish, while Si–Si bond lengths would lengthen and ∠Si–Si–Si bond angles would decrease (Fig. 3). And the relaxation of Si_0 contributes the most to ΔQ, which can be found in the percentage of ΔQ_{Si_0} in the ΔQ (Table 1).

The energy levels of the P_{b0} and P_{b1} defects before and after hole (electron) capture are all determined by examining the density of states (DOS), as shown in Fig. 4. The Si_0 atom contributes the most to the defect energy level, when the neutral defect captures a hole (electron), the magnetic moment becomes zero due to the unpaired electron in the dangling bond would vanish (pair).

Table 1. The change of Si–Si bond lengths, ∠Si–Si–Si bond angles and mass-weighted distortions of Si atom with a dangling bond ΔQ_{Si_0} and all atoms ΔQ for P_{b0} and P_{b1} defects by capturing hole or electron.

System	Si–Si (Å)			∠Si–Si–Si (°)			ΔQ_{Si_0} (amu$^{1/2}$·Å)	ΔQ (amu$^{1/2}$·Å)	$\Delta Q_{Si_0}/\Delta Q$ (%)
P_{b0}	2.382	2.334	2.356	112.13	115.31	107.55			
P_{b0}^{+}	2.371	2.306	2.346	118.56	120.42	114.87	1.944	2.559	75.97
P_{b0}^{-}	2.391	2.380	2.395	102.69	106.74	96.25	2.129	2.901	73.39
P_{b1}	2.366	2.321	2.279	118.53	107.11	109.04			
P_{b1}^{+}	2.380	2.311	2.245	123.50	114.87	118.03	2.581	4.076	63.32
P_{b1}^{-}	2.378	2.369	2.331	107.14	97.85	96.74	2.356	3.231	72.92

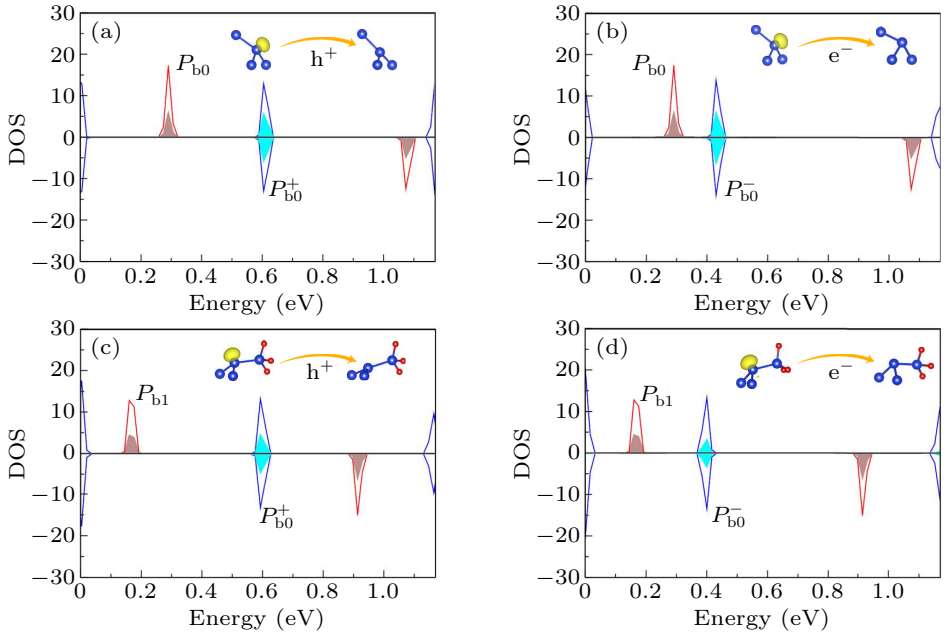


Fig. 4. Spin-polarized local density of state (LDOS) of P_{b0} defects (a) by capturing a hole and (b) by capturing an electron, P_{b1} defects (c) by capturing a hole and (d) by capturing an electron. The red and blue lines represent defect levels before and after hole (electron) capture, respectively. The brown and cyan regions represent DOS projection to Si atom with a dangling bond. The energy level of valence-band maximum (VBM) is set to 0 eV.

3.2. The carrier capture properties for P_{b0} defect and P_{b1} defect

The P_{b0} and P_{b1} defects are amphoteric defects, which act as both a donor and an acceptor state in the bandgap of Si. The complete non-radiative recombination is a sequence of electron-hole pair capture processes. Associated with the $(+/0)$ transition level, there are two capture processes: hole (p) capture for the neutral state (C_p^0) and electron (n) capture for the positively charged state (C_n^+). Similarly, there are also two capture processes involved in the $(0/-)$ transition level: electron capture for the neutral state (C_n^0) and hole capture for the negatively charged state (C_p^-). The 1D configuration coordinate diagram is used to analyze the capture processes. The relative parameters to describe the temperature dependence of carrier capture coefficients are shown in Table 1.

For the P_{b0} defect, the $(+/0)$ and $(0/-)$ transition levels are 0.26 eV and 0.79 eV above the VBM (i.e., ΔE are 0.26 eV and 0.38 in hole and electron capture for neutral state, respectively), respectively, which accords with the experimental results that the defect levels of the P_{b0} defect are broadly distributed with $(+/0)$ transition level approximately 1/3 eV below the middle of the band gap and the $(0/-)$ transition level approximately 1/3 eV above the middle of the band gap.[4] Figure 5(a) shows the configuration coordinate diagram for the transition between P_{b0} and P_{b0}^{+}, the equilibrium configuration of P_{b0}^{+} and P_{b0} correspond to $Q = 0$ and $Q = \Delta Q$, respectively.

The energy barriers of hole capture ($\Delta E_{\rm p}^{0}$) and electron capture ($\Delta E_{\rm n}^{+}$) are 5.34 meV and 199.53 meV, respectively, $\Delta E_{\rm p}^{0}$ is much smaller than $\Delta E_{\rm n}^{+}$, indicating that the hole capture process for the neutral state is faster than the electron capture process for the positively charged state and smaller temperature dependence of carrier capture coefficient. Figure 5(b) shows the similar results for the transition between $P_{\rm b0}$ and $P_{\rm b0}^{-}$, the energy barriers $\Delta E_{\rm n}^{0}$ and $\Delta E_{\rm p}^{-}$ are 0.52 meV and 230.14 meV, respectively, indicating that the electron capture process for the neutral state is also faster than the hole capture process for the negatively charged state.

The carrier capture coefficients as a function of temperature are depicted in Fig. 5(c), which includes the electron–phonon coupling and the overlap of potential energy surfaces. And the total non-radiative carrier capture coefficient ($C_{\rm tot}$) under steady-state conditions[33–35] can be derived as

$$C_{\rm tot} = \frac{C_{\rm n}^{0} + C_{\rm p}^{0}}{1 + C_{\rm n}^{0}/C_{\rm p}^{-} + C_{\rm p}^{0}/C_{\rm n}^{+}}. \tag{12}$$

As shown in Fig. 5(c), $C_{\rm p}^{0}$ and $C_{\rm n}^{0}$ are weakly dependent on temperature, but $C_{\rm n}^{+}$ and $C_{\rm p}^{-}$ show a strong temperature dependence. And $C_{\rm p}^{0}$ and $C_{\rm n}^{0}$ are higher than $C_{\rm n}^{+}$ and $C_{\rm p}^{-}$ at the low temperatures, which is consistent with the energy barriers. Because of the fact that $C_{\rm p}^{0} \gg C_{\rm n}^{0}$ and $C_{\rm p}^{0}/C_{\rm n}^{+} \gg 1 + C_{\rm n}^{0}/C_{\rm p}^{-}$, the total capture coefficient is approximately equal to $C_{\rm p}^{0}/(C_{\rm p}^{0}/C_{\rm n}^{+})$, i.e., $C_{\rm n}^{+}$, indicating that $C_{\rm tot}$ is limited by the electron capture process for positively charged state. At room temperature, $C_{\rm tot}$ of $P_{\rm b0}$ defect is about 1.25×10^{-8} cm^2/s, thus the non-radiative recombination coefficient (A) of $P_{\rm b0}$ defect can be derived by $A_{P_{\rm b0}} = N_{P_{\rm b0}} C_{\rm p}^{0} = 6.25 \times 10^{4}$ s^{-1}, which $N_{P_{\rm b0}}$ is the defect density of $P_{\rm b0}$ defect.

The $P_{\rm b1}$ defect is also one of the most dominating defects in a-SiO$_2$/Si(100), the $(+/0)$ and $(0/-)$ transition levels are 0.48 eV and 0.86 eV above the VBM (i.e., ΔE are 0.48 eV and 0.31 in hole and electron capture for neutral state, respectively), respectively, which accord with the experimental results.[32] Figures 6(a) and 6(b) show the configuration coordinate diagram for the transition between $P_{\rm b1}$ and $P_{\rm b1}^{+}$, and the transition between $P_{\rm b1}$ and $P_{\rm b1}^{-}$. The energy barriers $\Delta E_{\rm p}^{0}$, $\Delta E_{\rm n}^{+}$, $\Delta E_{\rm n}^{0}$ and $\Delta E_{\rm p}^{-}$ are 4.00 meV, 37.20 meV, 1.97 meV, and 264.03 meV, respectively, only $\Delta E_{\rm p}^{-}$ has a large value, indicating that the hole capture process for the negatively charged state is slower than other capture processes, and show a strong temperature dependence. As shown in Fig. 6(c), $C_{\rm p}^{0}$, $C_{\rm n}^{+}$ and $C_{\rm n}^{0}$ are indeed almost unchanged with increasing temperature, and higher than $C_{\rm p}^{-}$. At low temperature, $C_{\rm p}^{0}/C_{\rm n}^{+} \gg 1 + C_{\rm n}^{0}/C_{\rm p}^{-}$, thus leading that $C_{\rm tot} \approx C_{\rm p}^{0}/(C_{\rm n}^{0}/C_{\rm p}^{-})$, and as the temperature gets higher, the ratio of $C_{\rm n}^{0}/C_{\rm p}^{-}$ is gradually increased and even exceed $C_{\rm p}^{0}/C_{\rm n}^{+}$, making that $C_{\rm tot}$ approach gradually $C_{\rm n}^{+}$. Because of the smaller temperature dependence of $C_{\rm p}^{0}$, $C_{\rm n}^{0}$ and $C_{\rm n}^{+}$, $C_{\rm tot}$ is mainly influenced by $C_{\rm p}^{-}$, the variation tendency of $C_{\rm tot}$ with temperature is almost consistent with $C_{\rm p}^{-}$. At room temperature, $C_{\rm tot}$ of $P_{\rm b1}$ defect is about 1.90×10^{-8} cm^2/s, and the non-radiative recombination coefficient (A) of $P_{\rm b1}$ defect $A_{P_{\rm b1}} = 1.90 \times 10^{4}$ s^{-1}. $A_{P_{\rm b0}}$ and $A_{P_{\rm b1}}$ have the same order of magnitude, implying that both $P_{\rm b0}$ and $P_{\rm b1}$ defects are the dominant non-radiative recombination center in the interface of a-SiO$_2$/Si(100).

Table 2. The key parameters relative to carrier capture coefficients for $P_{\rm b0}$ and $P_{\rm b1}$ defects: mass-weighted deformation ΔQ, energies difference between adjacent vibrational energy levers $\hbar\omega_{\rm i,f}$, Huang–Phys factor $S_{\rm i,f}$, ionization energy ΔE, electron–phonon coupling matrix $W_{\rm if}$, and the surface areas of the supercell $S = 236$ Å^2 in first-principles calculation.

Reaction	ΔQ (amu$^{1/2}$·Å)	$\hbar\omega_{\rm i}$ (meV)	$\hbar\omega_{\rm f}$ (meV)	ΔE (eV)	$S_{\rm i}$	$S_{\rm f}$	$W_{\rm if}$ (eV/amu$^{1/2}$·Å)
$P_{\rm b0} + {\rm h}^{+} \rightarrow P_{\rm b0}^{+}$	2.559	21.40	21.68	0.26	16.78	17.00	6.04×10^{-4}
$P_{\rm b0}^{+} + {\rm e}^{-} \rightarrow P_{\rm b0}$	2.559	21.68	21.40	0.91	17.00	16.78	9.12×10^{-5}
$P_{\rm b0} + {\rm e}^{-} \rightarrow P_{\rm b0}^{-}$	2.901	19.18	19.94	0.38	18.63	19.37	4.15×10^{-5}
$P_{\rm b0}^{-} + {\rm h}^{+} \rightarrow P_{\rm b0}$	2.901	19.94	19.18	0.79	19.37	18.63	2.70×10^{-4}
$P_{\rm b1} + {\rm h}^{+} \rightarrow P_{\rm b1}^{+}$	4.076	14.90	16.69	0.48	28.57	32.00	4.90×10^{-4}
$P_{\rm b1}^{+} + {\rm e}^{-} \rightarrow P_{\rm b1}$	4.076	16.69	14.90	0.69	32.00	28.57	4.05×10^{-5}
$P_{\rm b1} + {\rm e}^{-} \rightarrow P_{\rm b1}^{-}$	3.231	17.95	19.05	0.31	21.62	22.95	1.16×10^{-4}
$P_{\rm b1}^{-} + {\rm h}^{+} \rightarrow P_{\rm b1}$	3.231	19.05	17.95	0.86	22.95	21.62	5.93×10^{-5}

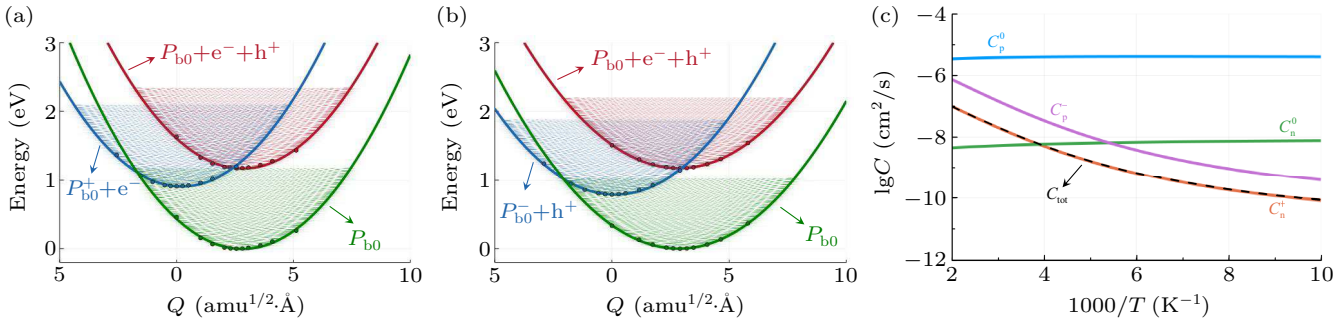


Fig. 5. Calculated 1D configuration coordinate diagrams for the transition between (a) $P_{\rm b0}$ and $P_{\rm b0}^{+}$, (b) $P_{\rm b0}$ and $P_{\rm b0}^{-}$. (c) Non-radiative capture coefficients of $P_{\rm b0}$ defect as a function of reciprocal temperature.

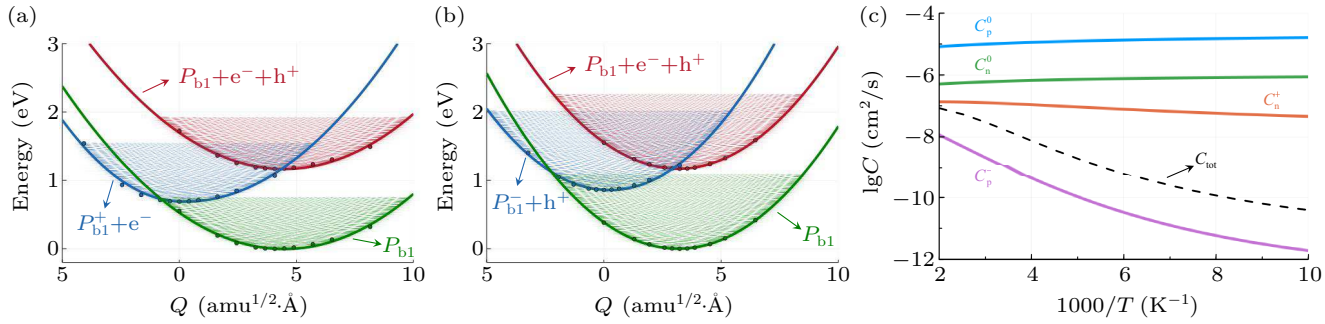


Fig. 6. Calculated 1D configuration coordinate diagrams for the transition between (a) P_{b1} and P_{b1}^+, (b) P_{b1} and P_{b1}^-. (c) Non-radiative capture coefficients of P_{b1} defect as a function of reciprocal temperature.

4. Conclusion

In summary, we use first principles calculations and the 1D static coupling approach to investigate the carrier capture properties of P_{b0} and P_{b1} defects, the existence of initial dangling bonds, making these defects to capture holes or electrons easily to eliminate the dangling bonds. Because of the bigger hole capture coefficients for neutral states, the P_{b0} and P_{b1} defects have a stronger capacity to capture holes than electrons, and the large non-radiative recombination coefficient further indicates that these defects are the non-radiative recombination center. The present study further demonstrates how reducing the formation and suppressing the activity of these defects will be key to maintaining device performance in the future.

Acknowledgments

Project supported by the Science Challenge Project (Grant No. TZ2016003-1-105), Tianjin Natural Science Fundation (Grant No. 20JCZDJC00750), and the Fundamental Research Funds for the Central Universities, Nankai University (Grant Nos. 63211107 and 63201182).

References

[1] Lenahan P M and Dressendorfer P V 1984 *J. Appl. Phys.* **55** 3495
[2] Gerardi G J, Poindexter E H, Caplan P J and Johnson N M 1986 *Appl. Phys. Lett.* **49** 348
[3] Vishnubhotla L, Chen W L and Ma T P 1990 *Appl. Phys. Lett.* **57** 1778
[4] Lenahan P M 2003 *Microelectron Eng.* **69** 173
[5] Caplan P J, Poindexter E H, Deal B E and Razouk R R 1979 *J. Appl. Phys.* **50** 5847
[6] Nishi Y 1971 *Jpn. J. Appl. Phys.* **10** 52
[7] Nishi Y, Tanaka K and Ohwada A 1972 *Jpn. J. Appl. Phys.* **11** 85
[8] Poindexter E H, Caplan P J, Deal B E and Razouk R R 1981 *J. Appl. Phys.* **52** 879
[9] Li P, Song Y and Zuo X 2019 *Phys Status Solidi Rapid Res Lett* **13** 1800547
[10] Schwank J R, Shaneyfelt M R, Fleetwood D M, Felix J A, Dodd P E, Paillet P and Ferlet-Cavrois V 2008 *IEEE Trans. Nucl. Sci.* **55** 1833
[11] Alkauskas A, Deák P, Neugebauer J, Pasquarello A and Van de Walle C G 2011 *Advanced Calculations for Defects in Materials: Electronic Structure Methods* (Chichester: John Wiley and Sons) p. 9
[12] Freysoldt C, Grabowski B, Hickel T, Neugebauer J, Kresse G, Janotti A and Van de Walle C G 2014 *Rev. Mod. Phys.* **86** 253
[13] Freed K F and Jortner J 1970 *J. Chem. Phys.* **52** 6272
[14] Marcus R A 1993 *Rev. Mod. Phys.* **65** 599
[15] Nan G J, Yang X D, Wang L J, Shuai Z G and Zhao Y 2009 *Phys. Rev. B* **79** 115203
[16] Pässler R 1974 *Czechoslov. J. Phys.* **24** 322
[17] Pässler R 1982 *Czechoslov. J. Phys.* **32** 846
[18] Alkauskas A, Yan Q M and Van de Walle C G 2014 *Phys. Rev. B* **90** 075202
[19] Kresse G and Furthmüller J 1996 *Phys. Rev. B* **54** 11169
[20] Kresse G and Joubert D 1999 *Phys. Rev. B* **59** 1758
[21] Blöchl P E 1994 *Phys. Rev. B* **50** 17953
[22] Perdew J P, Chevary J A, Vosko S H, Jackson K A, Pederson M R, Singh D J and Fiolhais C 1992 *Phys. Rev. B* **46** 6671
[23] Perdew J P and Wang Y 1992 *Phys. Rev. B* **45** 13244
[24] Li P, Chen Z H, Yao P, Zhang F J, Wang J W, Song Y and Zuo X 2019 *Appl. Surf. Sci.* **483** 231
[25] Heyd J, Scuseria G E and Ernzerhof M 2003 *J. Chem. Phys.* **118** 8207
[26] Yao P, Song Y and Zuo X 2021 *J. Phys. Chem. C* **125** 15044
[27] Komsa H P and Pasquarello A 2013 *Phys. Rev. Lett.* **110** 095505
[28] Freysoldt C, Neugebauer, J and Van de Walle C G 2009 *Phys. Rev. Lett.* **102** 016402
[29] Giustino F and Pasquarello A 2005 *Phys. Rev. B* **71** 144104
[30] Huang K and Rhys A 1950 *Proc. Math. Phys. Eng. Sci.* **204** 406
[31] Stirling A, Pasquarello A, Charlier J C and Car R 2000 *Phys. Rev. Lett.* **85** 2773
[32] Stesmans A and Afanas'ev V V 1998 *J. Phys.: Condens. Matter* **10** L19
[33] Alkauskas A, Dreyer C E, Lyons J L and Van de Walle C G 2016 *Phys. Rev. B* **93** 201304
[34] Zhang X, Turiansky M E, Shen J X and Van de Walle C G 2022 *J. Appl. Phys.* **131** 090901
[35] Zhang X and Wei S H 2022 *Phys. Rev. Lett.* **128** 136401